Physics

Physics Research Publications

Purdue University *Year* 2010

Surface and bulk electronic structures of LaFeAsO studied by angle-resolved photoemission spectroscopy

L. X. Yang, B. P. Xie, Y. Zhang, C. He, Q. Q. Ge, X. F. Wang, X. H. Chen, M. Arita, J. Jiang, K. Shimada, M. Taniguchi, I. Vobornik, G. Rossi, J. P. Hu, D. H. Lu, Z. X. Shen, Z. Y. Lu, and D. L. Feng

Surface and bulk electronic structures of LaFeAsO studied by angle-resolved photoemission spectroscopy

L. X. Yang,[1] B. P. Xie,[1,*] Y. Zhang,[1] C. He,[1] Q. Q. Ge,[1] X. F. Wang,[2] X. H. Chen,[2] M. Arita,[3] J. Jiang,[3] K. Shimada,[3] M. Taniguchi,[3] I. Vobornik,[4] G. Rossi,[4,5] J. P. Hu,[6] D. H. Lu,[7] Z. X. Shen,[7] Z. Y. Lu,[8] and D. L. Feng[1,†]

[1]*State Key Laboratory of Surface Physics, Department of Physics, and Advanced Materials Laboratory, Fudan University, Shanghai 200433, People's Republic of China*

[2]*Hefei National Laboratory for Physical Sciences at Microscale and Department of Physics, University of Science and Technology of China, Hefei, Anhui 230026, People's Republic of China*

[3]*Hiroshima Synchrotron Radiation Center and Graduate School of Science, Hiroshima University, Hiroshima 739-8526, Japan*

[4]*CNR-INFM, TASC Laboratory, AREA Science Park, Basovizza, 34012 Trieste, Italy*

[5]*Dipartimento di Fisica, Universita di Modena e Reggio Emilia, Via Campi 213/A, I-41100 Modena, Italy*

[6]*Department of Physics, Purdue University, West Lafayette, Indiana 47907, USA*

[7]*Stanford Synchrotron Radiation Lightsource, SLAC National Accelerator Laboratory, 2575 Sand Hill Road, Menlo Park, California 94025, USA*

[8]*Department of Physics, Renmin University of China, Beijing 100872, People's Republic of China*

(Received 13 June 2010; revised manuscript received 15 August 2010; published 23 September 2010)

The electronic structure of LaFeAsO, a parent compound of iron-arsenic superconductors, is studied by angle-resolved photoemission spectroscopy. By examining its dependence on photon energy, polarization, and sodium dosing, both the bulk and the surface contributions are identified. We find that a bulk band moves toward high binding energies below the structural transition temperature, and shifts smoothly across the spin-density-wave transition by about 25 meV. Our data suggest that the band reconstruction may play a crucial role in the spin-density-wave and the structural transitions. For the surface states, both the LaO-terminated and FeAs-terminated components are revealed. Certain small band shifts are observed for the FeAs-terminated surface states in the spin-density-wave state, which might be a reflection of the bulk electronic-structure reconstruction. Moreover, sharp quasiparticle peaks quickly rise at low temperatures, indicating drastic reduction in the scattering rate. A kink structure in one of the surface band is shown to be possibly related to the enhanced electron-phonon interactions on the polar surface.

DOI: 10.1103/PhysRevB.82.104519 PACS number(s): 74.25.Jb, 74.70.−b, 79.60.−i, 71.20.−b

I. INTRODUCTION

The discovery of superconductivity in $LaFeAsO_{1-x}F_x$ has declared the advent of iron-based high-temperature superconductors (Fe-HTSCs).[1–3] After intensive research, the record superconductivity transition temperature (T_c) of Fe-HTSCs is still held by the so called 1111 series.[4,5] Resembling the cuprates, superconductivity emerges from the antiferromagnetic ordered ground state upon proper doping.[2,3,6,7] The intimate relationship between superconductivity and magnetism makes it critical to study the magnetic properties in the parent compounds. On the other hand, the isotope effects on superconductivity and spin density wave,[8] and the kinks in band dispersions,[9,10] along with the ubiquitous cooccurrence of the structural and magnetic transitions, allude to the relevance of the lattice degree of freedom for the Fe-HTSC physics. In the parent compounds of 1111 series, the structural and spin-density-wave (SDW) transition temperatures are separated,[11] which provides an opportunity to reveal the origin of the structural transition and its influence on the electronic structure.

Angle-resolved photoemission spectroscopy (ARPES) has been employed to study the electronic structure of various Fe-HTSCs, revealing the electronic structure, superconducting gap, and the electron-boson coupling.[12–20] However, due to the covalent *Ln*-O bonding, *Ln*FeAsO (*Ln*=La, Sm, Ce, etc.) exposes a polar surface with charge redistribution after cleavage.[10,12,21,22] There are two types of surfaces, the *Ln*O-terminated and FeAs-terminated. A recent detailed band calculation of LaFeAsO shows that the electronic structure of the two types of surfaces deviates strongly from each other and from that of the bulk.[23] Since ARPES is essentially a surface probe, the measured band structure is strongly complicated by the surface states. Therefore, the bulk electronic structure of *Ln*FeAsO is still not definite. This prevents the understanding of this very first and probably the highest T_c series of iron pnictides, which in turn hampers the construction of a global picture of electronic structure in iron pnictides.

In this paper, we report the ARPES measurements of the electronic structure of LaFeAsO, a parent compound of the 1111 series of iron pnictides. By carefully conducting photon energy, polarization, and Na-dosing dependence studies on the complicated electronic structure, we could distinguish states from the bulk and the surface. As a result, the nature of the SDW state is exposed by the bulk band reconstruction at low temperatures. Similar to $BaFe_2As_2$ and other members in the so called 122 series,[16–19] no energy gap related to nesting is observed at the Fermi surfaces of LaFeAsO. Instead, a band at high binding energies shifts down as much as 25 meV, starting from the structural transition temperature and going through the SDW transition smoothly. This has been observed recently in NaFeAs by the authors,[24] where the fluctuating magnetic order was shown to appear below the

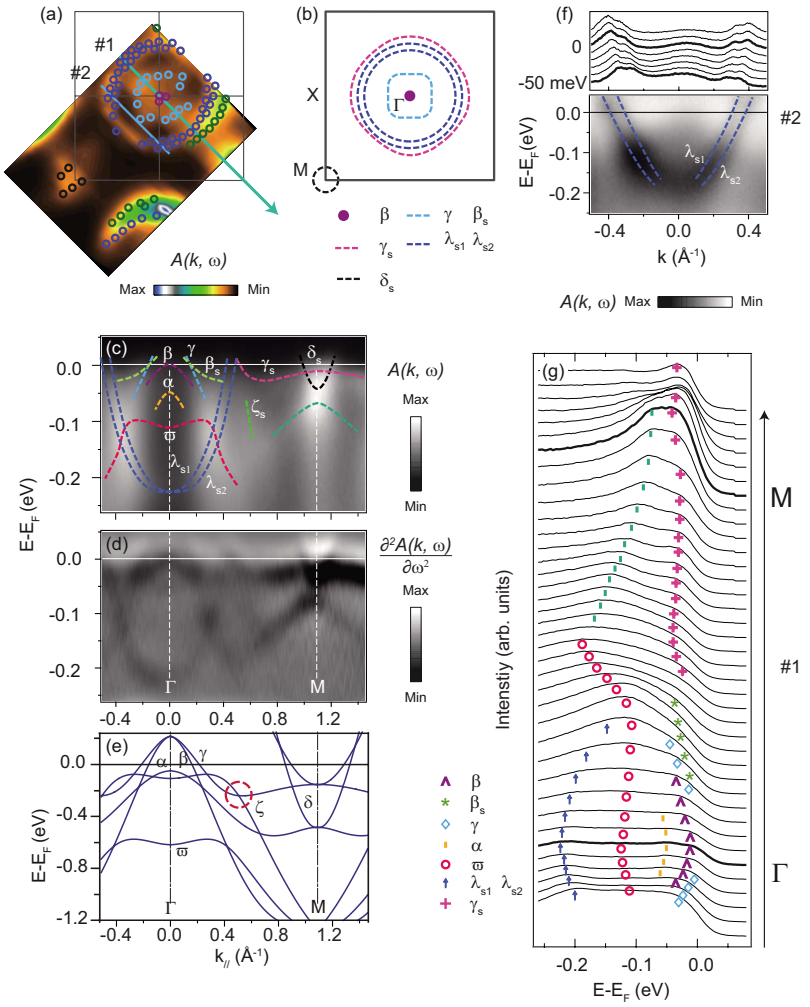

FIG. 1. (Color online) Fermi-surface mapping and band structure of LaFeAsO along Γ-M in the normal state (170 K). (a) ARPES intensity map in the Brillouin zone (BZ) integrated over ±5 meV around the Fermi energy (E_F), overlaid by the Fermi crossings. (b) The Fermi surfaces are constructed by tracking the Fermi crossings. (c) Photoemission intensity plot along Γ-M (cut 1 in panel a). The dashed curves are the guides to eyes obtained by tracking the local minimum locus of second derivative of the raw data with respect to energy as shown in panel d. (e) The calculated bulk electronic structure of LaFeAsO along Γ-M based on density functional theory. (f) The MDC's (upper panel) and photoemission intensity plot divided by the resolution convoluted Fermi-Dirac function (lower panel) along cut 2 as marked in panel a. (g) The corresponding EDCs along Γ-M. Data were taken using 24 eV circularly polarized photons.

structural transition temperature. Our results on LaFeAsO further suggest that the SDW picture established in the 122 and 111 series applies in the 1111 series as well. The reconstruction of the band structure at low temperatures effectively saves the total energy of the system and thus plays a crucial role in driving the SDW transition. Furthermore, we observed drastically rising coherent quasiparticle peaks, which indicates that scattering is strongly suppressed at low temperatures. A pronounced kink in dispersion is observed as well, suggesting possible importance of the electron-phonon interactions in the iron pnictides.[9,10]

II. EXPERIMENTAL

High-quality LaFeAsO single crystals were synthesized by NaAs-flux method as described elsewhere.[25] Resistivity data confirmed the SDW transition at T_N=138 K.[11] ARPES measurements were conducted at Beamline 9 of Hiroshima synchrotron radiation center (HSRC) with circularly polarized photons and a Scienta R4000 electron analyzer. The polarization and photon-energy dependence measurements were performed at Beamline 1 of HSRC and the APE Beamline in Elettra synchrotron light source. The energy resolution is 9 meV at Beamline 9, and 20 meV at Beamline 1 and APE, respectively. The overall angular resolution is about 0.3°. All samples were cleaved *in situ* and the ARPES measurements were carried out under ultrahigh vacuum better than 3.0×10^{-11} mbar at Beamline 9 and 5×10^{-11} mbar at Beamline 1 of HSRC. Data were taken within 6 h after cleavage to minimize the aging effect.

The energies of photons in the experiments range from 19 to 64 eV, which gives an electron escape depth of about 5–10 Å according to the universal mean-free-path curve for electron inelastic scattering in solids.[26] This corresponds to the first two or three layers of LaO or FeAs plane in LaFeAsO. An inner potential of 16 eV is chosen to determine the k_z of the high symmetry points of the Brillouin zone in the photon-energy dependence studies.

III. DATA ANALYSIS AND DISCUSSION

A. Normal-state electronic structure

The electronic structure in the normal state (170 K) is presented in Fig. 1. Photoemission intensities are integrated over a [−5 meV, +5 meV] window around the Fermi energy (E_F) to acquire Fermi surface as shown in Figs. 1(a) and 1(b). The observed Fermi surface consists of three hole pockets, two electron pockets and a tiny patch like feature around the Γ point as well as one electron pocket around M. This is very different from the calculated bulk electronic structure

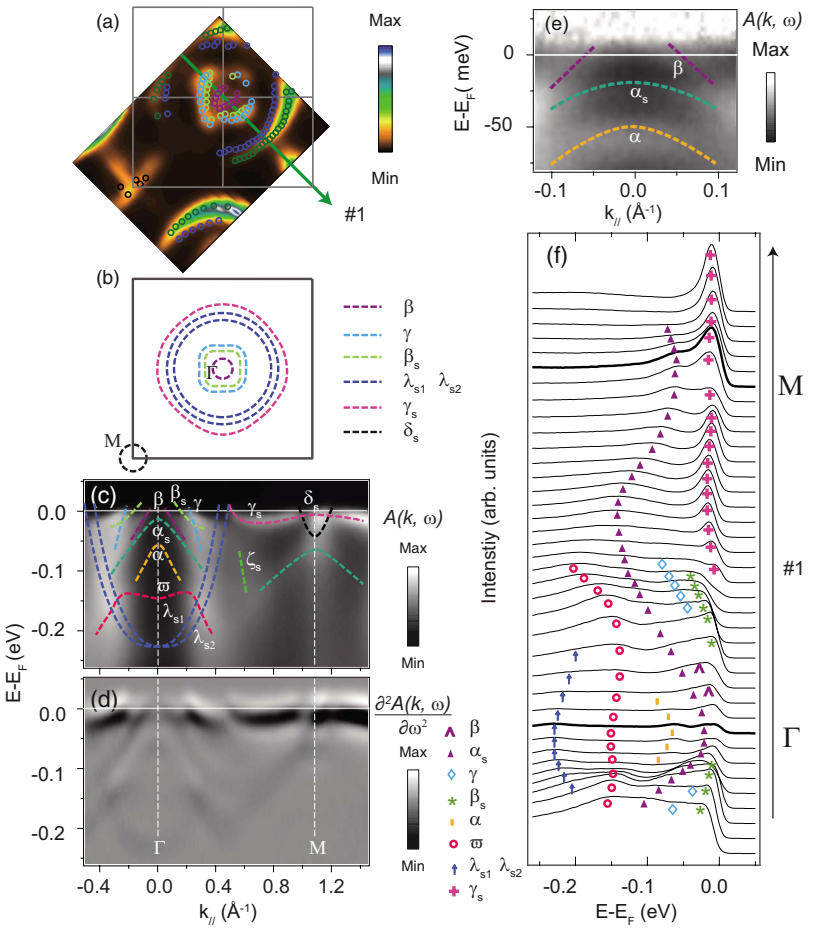

FIG. 2. (Color online) Fermi-surface mapping and band structure along Γ-M of LaFeAsO in the SDW state (10 K). (a) ARPES intensity map in the BZ integrated over ±5 meV around the E_F, overlaid by the Fermi crossings. (b) The Fermi surfaces are constructed by tracking the Fermi crossings. (c) Photoemission intensity plot along Γ-M (cut 1 in panel a). The dashed curves are the guides to eyes obtained by tracking the local minimum locus of second derivative of the raw data with respect to energy as shown in panel d. (e) The photoemission intensity plot after each MDC is normalized by its integrated weight. (f) The corresponding EDCs along Γ-M. Data were taken using 24 eV circularly polarized photons.

and what is observed in other iron pnictides.[27,28] The band structure as indicated by the dashed curves in Fig. 1(c) is resolved by tracking the local minimum locus in the second derivative of the ARPES intensity plot with respect to energy [Fig. 1(d)] and confirmed by the peaks in the corresponding energy distribution curves (EDCs) as shown in Fig. 1(g). The top of the β band touches the E_F and forms a Fermi patch near Γ. The Fermi crossings of γ and β_s nearly coincide, forming two nearly coincident hole pockets of the Fermi surface. Two parabolic electron bands λ_{s1} and λ_{s2} contribute two electron Fermi pockets around Γ. A weak but resolvable feature α shows up with its top at about 50 meV below E_F. The flat γ_s band contributes one large hole pocket around Γ which is much larger than the corresponding bulk Fermi surface in the calculation. Around the M point, only one electron band could be clearly resolved instead of two in the calculations, which could be due to the Matrix element effects. Another electronlike band could be resolved using linearly polarized photons as shown in Figs. 3(i), 1, 3(i), and 2. Note that the petal-like feature around M in Fig. 1(a) stems from the remnant spectral weight of the flat γ_s band, instead of Fermi crossings.

The overall measured electronic structure of LaFeAsO deviates strongly from that of other pnictides and the calculations as shown in Fig. 1(e).[16,27–29] In total, we observed nine bands and five Fermi surface sheets around Γ (actually, another holelike band α_s could be resolved around Γ at low temperature as shown below), much more than that in the bulk band calculations. This complication can be qualitatively explained by the recent calculations of the surface and bulk electronic structures of LaFeAsO.[23] Due to the strong La-O and Fe-As covalent bonding, the surface is either an FeAs or a LaO plane. The polarity of the surface causes significant lattice relaxation and charge redistribution to minimize its static electric energy and thus changes the electronic structure dramatically.[12,13] As a result, the FeAs-terminated surface is electron deficient while the LaO-terminated surface is electron excess. The two types of surfaces could coexist on a single cleaved sample and the FeAs plane underneath the LaO-terminated surface is different from the FeAs-terminated surface, they conspire to construct the complicated band structure in the experimental data. Since ARPES probes only 5–10 Å with the photon energies exploited here, the measured electronic structure are mainly contributed by the states from the first two or three layers of LaO or FeAs planes.

The surface band calculations (Ref. 23) clearly predicted that the excess electrons in the surface LaO plane reside in the La $5d+6s$ states and give a large electron pocket around Γ. However, instead of one, we have observed two electron bands (λ_{s1} and λ_{s2}), which could be resolved more clearly in Fig. 1(f). Since the observed two bands mimic the spin-orbital splitting of the Au(111) surface states, the difference between our data and the predicted ones might be caused by the fact that spin-orbital coupling was not included in the calculation while the spin-orbital coupling of $5d$ electrons is

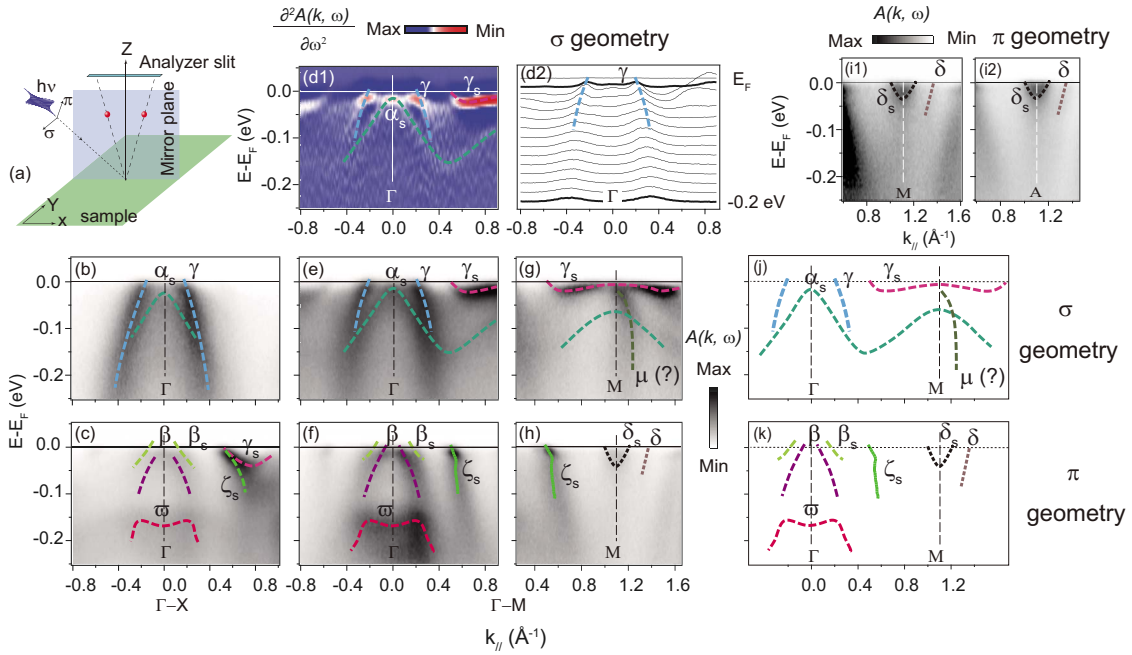

FIG. 3. (Color online) Polarization dependence measurements along high symmetry directions. (a) Schematic of two geometries of experimental setups. [(b) and (c)] ARPES intensity plots along Γ-X. (d1) The second derivative of ARPES intensity plot with respect to energy and (d2) the corresponding MDC's along Γ-M. [(e)–(h)] ARPES intensity plots along Γ-M. [(i1) and (i2)] ARPES intensity plots around the M and *A* points. The contrast of the images is adjusted to show the δ band more clearly. (j) and (k) summarize the band structure extracted for the corresponding polarizations. The dashed curves in the photoemission intensity plots are the guides to eyes while the solid curves are the fitting of MDC's peaks. The geometries of experimental setups are marked on the top or right of the panels. The corresponding photon energies for the Γ, M, and *A* points are 59 eV, 43 eV, and 33 eV, respectively, to reach the right k_z. Data were taken at 10 K.

not negligible.[30] For comparison, the momentum splitting of λ_{s1} and λ_{s2} is about 0.03 $Å^{-1}$ and the Rashba energy is merely ~1 meV. Correspondingly, the Rashba parameter α_R, i.e., the ratio of the Rashba energy to the momentum splitting, is about 0.023 eV $Å^{-1}$. This value is much smaller than that of Au: α_R=0.33 eV $Å^{-1}$ (Ref. 31) but comparable with that of the two-dimensional electronic system in the InGaAs/InAlAs heterostructure.[32] Furthermore, we note that the occupied bandwidth of λ_{s1} and λ_{s2} is about 0.22 eV, which is similar to the calculation (0.2 eV), indicating weak correlations in the LaO layer, in contrast to the FeAs bands.[33]

B. SDW state electronic structure

Figure 2 displays the corresponding electronic structure in the SDW state. For the Fermi surface as shown in Figs. 2(a) and 2(b), the tiny patchlike feature at Γ evolves into a small hole pocket. The Fermi crossings of the γ and β_s bands does not coincide any more, forming two hole pockets around the Γ point. The size of γ pocket expands about 70% at low temperature. There is little change in the other Fermi surface sheets. The band structure along Γ-M is shown in the ARPES intensity plot [dashed curves in Fig. 2(c)] and its second derivative with respect to energy [Fig. 2(d)]. An additional holelike band (α_s) with its band top at about −20 meV could be resolved in the Fig. 2(e). The reason that α_s was not resolved at high temperatures might be due to thermal broadening. The splitting of the λ_{s1} and λ_{s2} bands is independent of temperature, which is expected for spin orbital splitting. The α and ϖ bands move about 5 meV and roughly 30 meV downward, respectively, saving the total energy of the system. The γ_s band moves about 5 meV toward E_F, sharpening the petal-like feature around the M point without additional Fermi crossing of the γ_s band. No clear variation in the electron band around M is found. Moreover, no energy gap related to Fermi surface nesting was observed, similar to the case of the 122, 111, and 11 series.[16–19,24,33]

C. Polarization dependence

The multiband nature of the iron pnictides leads to complex band structure and the additional surface states make it even more complicated in LaFeAsO. Since the band structure shows strong polarization dependence, we conducted polarization dependent ARPES measurements to further resolve the band structure. Figure 3(a) displays the definition of two different experimental geometries according to the linear polarization of the incoming photons. The incident beam and the sample surface normal define a mirror plane. For the σ (or π) experimental geometry, the electric field of the incident photons is out of (or in) the mirror plane. The matrix element for the photoemission process could be described as

$$M_{f,i}^{\mathbf{k}} \propto |\langle \Psi_f^{\mathbf{k}} | \hat{\varepsilon} \cdot \mathbf{r} | \Psi_i^{\mathbf{k}} \rangle|^2.$$

Since the final state $\Psi_f^{\mathbf{k}}$ of photoelectrons could be approximated by a plane wave with its wave vector in the mirror plane, $\Psi_f^{\mathbf{k}}$ is always even respect to the mirror plane in our

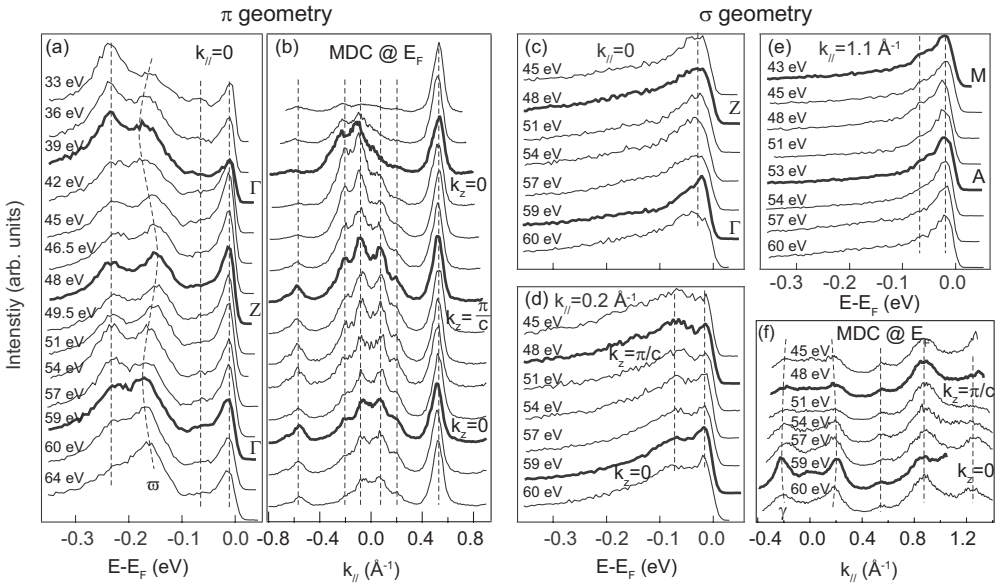

FIG. 4. Photon-energy dependence of (a) the EDCs at in-plane momentum $k_{\|}=0$ and (b) the MDC's at E_F. The EDCs at in-plane momentum (c) $k_{\|}=0$, (d) $k_{\|}=0.2$ Å^{-1}, and (e) $k_{\|}=1.1$ Å^{-1}. (f) The MDC's at E_F. Data in panels a and b were taken under π geometry while data in panels c–e were taken under σ geometry of experimental setup. The in-plane projection is along the Γ-M direction. Data were taken at 10 K.

experimental geometry. In the σ (or π) geometry, $\hat{\varepsilon}\cdot\mathbf{r}$ is odd (or even) with respect to the mirror plane. Thus, only the odd (or even) component of the initial state $\Psi_i^{\mathbf{k}}$ could show up in the photoemission data.[33]

The photoemission intensity plots along high symmetry directions are shown in Figs. 3(b), 3(c), and 3(e)–3(h). The dashed lines are the guides to eyes while the solid curves are the fitting of the momentum distribution curves (MDCs) peaks. Around the Γ point, the β and β_s (α_s and γ) bands only shows up in π (σ) geometry of experimental setup, exhibiting their even (odd) nature with respect to the mirror plane. The flat γ_s band is absent in σ (or π) geometry along Γ-X (or Γ-M). It exhibits different parity in two high symmetry directions. The ϖ band could be observed only in π geometry along both directions. Its parity is analogous to that of the d_{z^2} band as predicted in density functional theory.[33] Figure 3(d) and 1 shows that the α_s band disperses from Γ to M and connects smoothly with the holelike band there. Around the M point, another electron band δ is observed. The δ and δ_s bands only shows up in the π experimental geometry, indicating their even parities. The contrast of the ARPES intensity plots around M and *A* are adjusted to show the δ band more clearly in Figs. 3(i), 1, 3(i), and 2. Note that we observed a fast dispersed holelike band μ around the M point, whose origin is still not clear yet [Fig. 3(g)]. We have reproduced the obtained band structure under different experimental geometries in Figs. 3(j) and 3(k) to summarize the band structure along Γ-M.

An interesting result in Figs. 3(f) and 3(h) is the kinklike dispersion of the ζ_s band, which has been reported earlier in CeFeAsO as well.[10] The dispersion of the ζ_s band is tracked by fitting its MDCs (the green solid curves). A kink does appear at about 30 meV, which might indicate electron-phonon interactions for this particular band. However, band crossings could cause similar structure. Indeed, there might be a band crossing in this momentum region as highlighted by the red dashed circle in Fig. 1(e). A kink could be possibly introduced by the hybridization of the γ_s and ζ_s bands. In that case, the γ_s band should connect either to the γ or the β_s band to hybridize with the ζ_s band. However, the γ band could be clearly resolved to disperse quickly downward from the MDC's in Fig. 3(d) and 2, it could not connect to the γ_s band. On the other hand, β_s and γ_s have the opposite parities as shown in Figs. 3(j) and 3(k). Based on local density approximation calculations and our previous studies of the orbital nature of bands in $BaFe_{2-x}Co_xAs_2$,[34] a band should not change its parity in such a small momentum range. Therefore, β_s and γ_s bands could not be from the same band, either. In conclusion, the polarization data confirms that the kink is not caused by a band crossing but most likely intrinsic electron-phonon interactions.

D. Identification of surface and bulk electronic structure: k_z dependence and Na dosing effects

It is crucial to identify the bulk and surface bands to reveal the intrinsic response of the electronic structure to the phase transitions. Photon-energy dependence measurements were carried out for this purpose since different photon energies correspond to different k_z's and only bulk bands could exhibit k_z dispersion. Under the π geometry of experimental setup, as shown in Figs. 4(a) and 4(b), only the ϖ band has noticeable k_z dependence as its energy position at $k_{\|}=0$ changes with the variation in photon energy. Thus, it should be one of the bulk bands. No clear k_z dependence is observed for the bands crossing E_F according to the photon energy dependence of the MDC's at E_F as shown in Fig. 4(b). For the bands observed under σ experimental geometry, only weak k_z dependence could be verified for the γ band from the MDC's at E_F as shown in the Fig. 4(f). No other bands

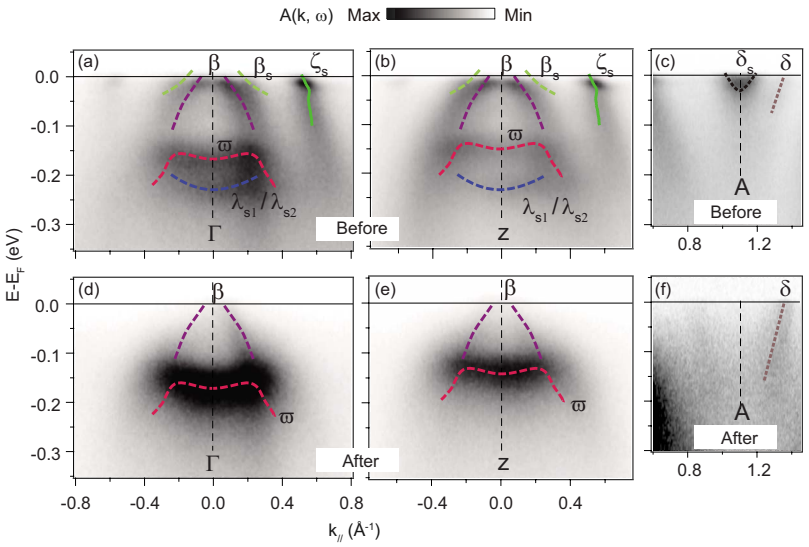

FIG. 5. (Color online) Photoemission intensity plots along (a) the Γ-M direction, (b) the Z-A direction, and (c) the A-Z direction. [(d)–(f)] After the sample was exposed to Na dosing, data were taken at the same condition as panels a–c. The dashed curves are the guides to eyes while the solid curves are the fitting of MDC's peaks. Data were taken at 10 K under π experimental geometry as in Fig. 3(a). The corresponding photon energies for the Γ, Z, and *A* points are 59 eV, 48 eV, and 33 eV, respectively.

show noticeable k_z dependence as shown by the EDCs at $k_\parallel=0$, $k_\parallel=1.1$ Å^{-1}, and $k_\parallel=0.2$ Å^{-1} [Figs. 4(c)–4(e)]. Considering the short electron escape depth, the bulk bands observed here are most likely originated from the FeAs plane below the LaO plane, for which the calculation indicates its carrier concentration is close to that of the bulk.[23] The k_z dispersion suggests that the band structure quickly becomes bulklike in the layer just underneath the surface.

For the bands that do not show much k_z dispersion, they could be from either surface or bulk in such a quasi-two-dimensional system. We further explore their reactions to the surface disorder effects through Na dosing, as the bulk bands are expected to be more robust than the surface ones. The sample was exposed to a Na evaporator at 150 °C for 10 s, which would put about 1 monolayer of Na atoms on the surface. Our data indicate that the chemical potential of the system is not changed too much after Na dosing. Thus, we would expect that additional scattering channels are introduced on the surface by the Na dosing, which would dramatically change the surface bands. The data taken in π geometry before and after the dosing are shown in Fig. 5. Indeed, many bands disappear, but the bulk ϖ band is barely changed by Na dosing. Since the ϖ band is mostly made of d_{z^2} orbital and still survives the sodium dosing, we assume that the other bulk bands made of those more "in-plane" orbital would survive as well. Consistently, the surface LaO band (λ_{s1} or λ_{s2}) disappear after Na dosing as shown in Figs. 5(a) and 5(c). The β_s and ζ_s bands disappear as well while the β band survives the dosing. Since the β band reacts to the Na dosing so differently from the surface bands, we attribute the β band to the bulk, while the β_s and ζ_s bands to the surface FeAs plane.

For the *A* point, only the δ band survives the dosing, while the δ_s band disappears after Na dosing as shown in Figs. 5(c) and 5(f), indicating their bulk and surface characters, respectively. In calculation, there should be four electron bands around M, two surface bands and two bulk bands. However, because of the electron deficiency on surface, one of the surface electron bands is not occupied. One of the bulk electronlike bands is missing in our data, probably due to its weak intensity or matrix element effects.

Due to the surface charge redistribution, calculation shows that the doping concentrations and band structures of the several layers close to surface are different from each other and that in bulk. The surface carrier concentration could be estimated by the Luttinger volume of the relevant Fermi surfaces. We identify three surface bands crossing Fermi level around Γ, which is consistent with the surface band calculation.[23] The carrier occupation of the surface β_s, γ_s, ζ_s, and δ_s bands is about $4.39e^-$ per $[Fe_2As_2]$ formula unit, smaller than the calculated $4.89e^-$ (based on the calculated Fermi surface in Ref. 23) and the expected $6e^-$ for the bulk bands.[13] On the other hand, the counting for the states of LaO layer gives rise to 0.53 excess electrons per $[La_2O_2]$ formula unit, larger than the calculated number of $0.25e^-$ (based on the calculated Fermi surface in Ref. 23). The certain difference may be related to the fact that some bands (thus some Fermi pockets) might be missing in the experiments.

E. Shifts in bulk band structure correlated with the SDW transition

The identified bulk bands allow us to investigate the intrinsic bulk response of the electronic structure to the phase transitions. The band structure in the normal state and SDW state are reproduced and overlaid in Fig. 6(a). The ϖ band clearly shifts roughly 30 meV to high energies, which reduces the total energy of the system effectively and energetically favors the SDW transition. The temperature dependence of EDCs at $k_\parallel=0.43$ Å^{-1} is tracked to examine the evolution of the ϖ band. As shown in Fig. 6(b), both the peak position and the leading edge corresponding to the ϖ band shift about 30 meV toward the high energies from 180 to 15 K. The shift starts around the structural transition temperature and goes through the SDW transition smoothly as shown in the inset of Fig. 6(b) and by the green triangles in Fig. 6(d). Since the dispersion of ϖ is concealed by other bands here, data taken with 19 eV photons are presented in Fig. 6(c), where the ϖ band is more enhanced due to certain matrix element effects. More accurately, the band shift as much as 25 ± 4 meV is quantified by both the peak positions

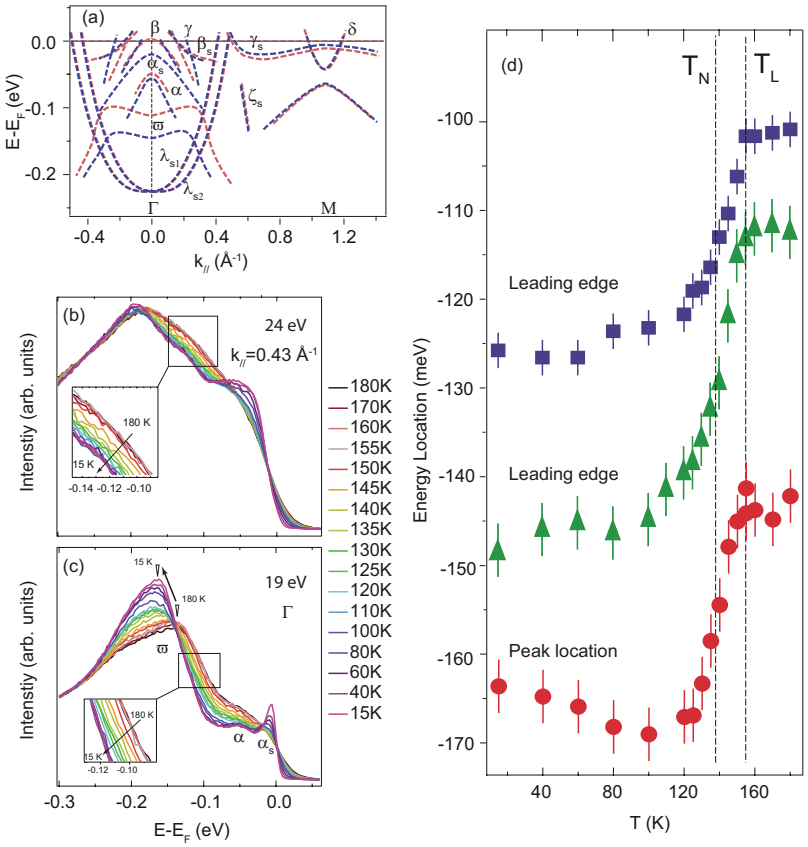

FIG. 6. (Color online) The band shift in LaFeAsO. (a) The comparison of the band structure at 170 K (red dashed curves) and 10 K (blue dashed curves) reproduced from Figs. 1 and 2. [(b) and (c)] The temperature dependence of EDCs at (b) $k_{\|}$=0.43 Å^{-1} obtained using 24 eV photons and (c) the Γ point obtained using 19 eV photons. The insets of panels b and c zoom in the rectangle region to show the leading edge shift more clearly. (d) The green triangles are the leading edge locations of the EDCs corresponding to the ϖ band in panel b. The blue squares and the red circles are the leading edge and peak locations of the EDCs corresponding to the ϖ band in panel c.

(red circles) and leading edge locations (blue squares) as shown in Fig. 6(d). The difference between the band shift obtained with 24 eV photons and 19 eV photons might be due to different k_z's. Data obtained in different ways all show that the band shift indeed starts from the structural transition and proceeds smoothly across the SDW transition to high energies.

This fact suggests that such band shift is related to the structural transition. However, the 0.52% distortion of the lattice could only account for about 4 meV band shift, which is far too less than the observation. On the other hand, the band shift could be related to the magnetic ordering considering its same energy scale as the magnetic exchange interactions.[16,17,19,24] Therefore, the smoothly evolution of the band shift across the SDW transition could be interpreted that there is already SDW fluctuation or short-range magnetic order at the structural transition temperature. Particularly, such a shift of band at the structural transition temperature has been observed in NaFeAs before.[24] Furthermore, it has been proved that a short-range magnetic order emerges around the structural transition temperature since the band folding due to such an order is observed starting from the structural transition temperature.[24] Therefore, the band shift in NaFeAs and LaFeAsO can be directly associated with the SDW fluctuations. Coincidentally, it has been proposed that the magnetic fluctuations could drive the structural transition.[35] Our result provides direct support for such a scenario in the 1111 series of iron pnictides. The observed shift of bands at high binding energies is consistent with the reconstruction of the electronic structure evolving into the SDW state in the parent compounds of 122 series.[16–19] Therefore, our observation of the band shift in LaFeAsO supports the electronic structure reconstruction as the mechanism for SDW transition. It might allude to the existence of an electronic nematic phase in the 1111 series between structural and SDW transitions as proposed in Ref. 35.

F. Drastic temperature dependence of quasiparticles

To further investigate the influences of the structural and SDW transitions on electronic structure, the sharp quasiparticle peaks at low temperatures as shown in Fig. 2(f) are examined as a function of temperature in Fig. 7. At the Γ point [Fig. 7(a)], prominent coherent quasiparticle peaks emerge as temperature decreases, suggesting a rapid decrease in the scattering rate. The same behavior could be found at a large portion of Brillouin zone, such as the M point and the location of $k_{\|}$=0.75 Å^{-1} [Figs. 7(b) and 7(c)]. The drastic rising of the quasiparticle peaks is well beyond the thermal sharpening effect at low temperatures. In order to reveal the relation between this anomalous evolution of the quasiparticle peaks and the phase transition, we divide the Fermi-Dirac functions of the temperature dependent EDCs in Fig. 7(c) and fit the quasiparticle peak with a Lorentz function and a linear background as shown in the inset of Fig. 7(c). The quasiparticle peak width which reflects the scattering rate decreases drastically at low temperatures as indicated by the red circles in Fig. 7(d). Consistently, the quasiparticle weight near E_F increases at low temperatures as shown in Fig. 7(d) (blue squares) Such decrease of scattering rate is compatible with that in CeFeAsO,[10] except that surface and bulk bands were not distinguished there.

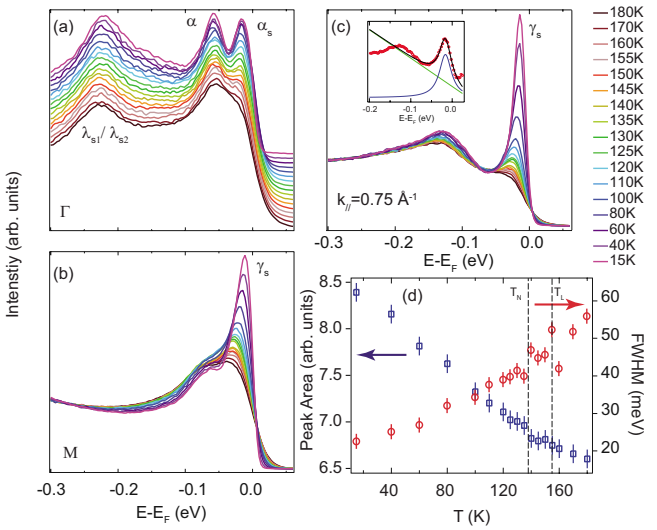

FIG. 7. (Color online) The evolution of the electronic structure in LaFeAsO. [(a)–(c)] Temperature dependence of EDCs with momentum locations at (a) Γ, (b) M, and (c) $k_{\|}$=0.75 Å^{-1}. The inset of panel c shows the fitting of the EDC at 100 K divided by the Fermi-Dirac function. (d) The evolution of the peak area (blue rectangles) and full width at half maximum (red circles) of the EDCs in the panel c. The peak area is obtained by integrating the spectral weight of the EDCs over a window of [−0.065, 0.05] eV.

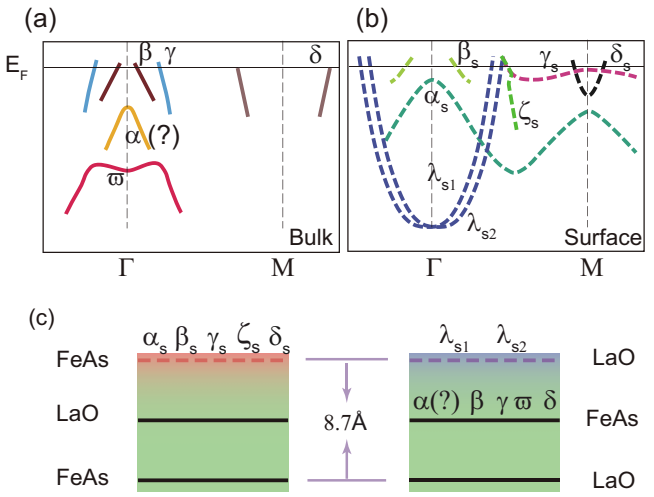

FIG. 8. (Color online) The summary of (a) the bulk and (b) the surface band structures that can be measured. (c) The diagram for the origin of the measured bands. The α band is assigned to the bulk because of its relatively high binding energies. But it is not confirmed by either the photon energy or the Na dosing dependence measurements.

No noticeable anomaly for the evolution of the peak width at phase transitions is observed although it is proposed that the dramatic decrease of the scattering rate is a signature of SDW transition.[10] However, Since the surface is still a quasi-two-dimensional system, it can be coupled to the bulk, for example, through certain scattering processes. Thus, the drastic temperature dependence of the surface bands might be related to the SDW transition in the bulk. The intrinsic relationship of this peculiar behavior and the phase transitions needs further studies. However, one of the possible explanation is that the magnetic fluctuations happen even above the structural transition and are suppressed by the formation of a spin gap as temperature is decreased, thus some of the scattering channels are eliminated. Indeed, such suppression of fluctuations at the low temperatures has been verified in $(Sr,Ba)Fe_2As_2$ by neutron scattering.[36,37] On the other hand, NMR measurements have verified the change in the fluctuation around structural transition and its suppression at low temperatures although there is a drastic enhancement of the fluctuations around SDW transition.[38,39]

IV. SUMMARY

To summarize, we have obtained a comprehensive picture of the electronic structure in LaFeAsO by distinguishing bulk [Fig. 8(a) curves] and surface bands [Fig. 8(b)]. The origin of the bands is summarized in Fig. 8(c) as well. We note that some certain bands may be missing in the measurements because of the matrix element effects. Due to the charge redistribution effect in the 1111 series, the measured electronic structure of LaFeAsO is heavily contaminated by the surface states. Therefore, great caution has to be taken on ARPES data obtained on this 1111 series of iron pnictides. For example, the measured superconducting gap on a surface band might be caused by the proximity effects, and the strong kink is actually on a surface band, it does not necessarily suggest strong electron-phonon interactions in the bulk bands.

Our data show that the large downward shift of the bulk band saves the total energy of the system and drives the phase transitions. The onset of this shift at the structural transition temperature further evidence the occurrence of a fluctuating magnetic ordered phase that might play a role in the structural transition. The results in the 1111 series are consistent with the observations in the 122 and 111 series of iron pnictides, suggesting the universality of the electronic response to the structural and magnetic phase transitions. Our results would help to construct a global picture of the Fe-HTSC physics.

ACKNOWLEDGMENTS

This work was supported by the NSFC, MOST (National Basic Research Program under Grants No. 2006CB921300 and No. 2006CB601002), MOE, and STCSM of China. Some preliminary data were taken at beam line 5–4 of Stanford Synchrotron Radiation Laboratory, which is operated by the DOE, Office of Basic Energy Science, Divisions of Chemical Sciences and Material Sciences.

*bpxie@fudan.edu.cn
†dlfeng@fudan.edu.cn

[1] Y. Kamihara, T. Watanabe, M. Hirano, and H. Hosono, J. Am. Chem. Soc. **130**, 3296 (2008).
[2] X. H. Chen, T. Wu, G. Wu, R. H. Liu, H. Chen, and D. F. Fang, Nature (London) **453**, 761 (2008).
[3] G. F. Chen, Z. Li, D. Wu, G. Li, W. Z. Hu, J. Dong, P. Zheng, J. L. Luo, and N. L. Wang, Phys. Rev. Lett. **100**, 247002 (2008).
[4] Z. A. Ren, W. Lu, J. Yang, W. Yi, X.-L. Shen, Z. Cai, G.-C. Che, X.-L. Dong, L.-L. Sun, F. Zhou, and Z.-X. Zhao, Chin. Phys. Lett. **25**, 2215 (2008).
[5] C. Wang, L.-J. Li, S. Chi, Z.-W. Zhu, Z. Ren, Y.-K. Li, Y.-T. Wang, X. Lin, Y.-K. Luo, S. Jiang, X.-F. Xu, G.-H. Cao, and Z. A. Xu, EPL **83**, 67006 (2008).
[6] H. Takahashi, K. Igawa, K. Arii, Y. Kamihara, M. Hirano, and H. Hosono, Nature (London) **453**, 376 (2008).
[7] M. Xu, F. Chen, C. He, H.-W. Ou, J.-F. Zhao, and D.-L. Feng, Chem. Mater. **20**, 7201 (2008).
[8] R. H. Liu, T. Wu, G. Wu, H. Chen, X. F. Wang, Y. L. Xie, J. J. Ying, Y. J. Yan, Q. J. Li, B. C. Shi, W. S. Chu, Z. Y. Wu, and X. H. Chen, Nature (London) **459**, 64 (2009).
[9] A. A. Kordyuk, V. B. Zabolotnyy, D. V. Evtushinsky, T. K. Kim, I. V. Morozov, M. L. Kulic, R. Follath, G. Behr, B. Buechner, and S. V. Borisenko, arXiv:1002.3149 (unpublished).
[10] H. Liu, G. F. Chen, W. Zhang, L. Zhao, G. Liu, T.-L. Xia, X. Jia, D. Mu, S. Liu, S. He, Y. Peng, J. He, Z. Chen, X. Dong, J. Zhang, G. Wang, Y. Zhu, Z. Xu, C. Chen, and X. J. Zhou, Phys. Rev. Lett. **105**, 027001 (2010).
[11] C. de la Cruz, Q. Huang, J. W. Lynn, J. Li, W. Ratcliff II, J. L. Zarestky, H. A. Mook, G. F. Chen, J. L. Luo, N. L. Wang, and P. Dai, Nature (London) **453**, 899 (2008).
[12] D. H. Lu, M. Yi, S.-K. Mo, A. S. Erickson, J. Analytis, J.-H. Chu, D. J. Singh, Z. Hussain, T. H. Geballe, R. R. Fisher, and Z.-X. Shen, Nature (London) **455**, 81 (2008).
[13] D. H. Lu, M. Yi, S.-K. Mo, J. G. Analytis, J.-H. Chu, A. S. Erickson, D. J. Singh, Z. Hussain, T. H. Geballe, I. R. Fisher, and Z.-X. Shen, Physica C **469**, 452 (2009).
[14] H. Ding, P. Richard, K. Nakayama, K. Sugawara, T. Arakane, Y. Sekiba, A. Takayama, S. Souma, T. Sato, T. Takahashi, Z. Wang, X. Dai, Z. Fang, G. F. Chen, J. L. Luo, and N. L. Wang, EPL **83**, 47001 (2008).
[15] P. Richard, T. Sato, K. Nakayama, S. Souma, T. Takahashi, Y.-M. Xu, G. F. Chen, J. L. Luo, N. L. Wang, and H. Ding, Phys. Rev. Lett. **102**, 047003 (2009).
[16] L. X. Yang, Y. Zhang, H. W. Ou, J. F. Zhao, D. W. Shen, B. Zhou, J. Wei, F. Chen, M. Xu, C. He, Y. Chen, Z. D. Wang, X. F. Wang, T. Wu, G. Wu, X. H. Chen, M. Arita, K. Shimada, M. Taniguchi, Z. Y. Lu, T. Xiang, and D. L. Feng, Phys. Rev. Lett. **102**, 107002 (2009).
[17] Y. Zhang, J. Wei, H. W. Ou, J. F. Zhao, B. Zhou, F. Chen, M. Xu, C. He, G. Wu, H. Chen, M. Arita, K. Shimada, H. Namatame, M. Taniguchi, X. H. Chen, and D. L. Feng, Phys. Rev. Lett. **102**, 127003 (2009).
[18] M. Yi, D. H. Lu, J. G. Analytis, J.-H. Chu, S.-K. Mo, R.-H. He, M. Hashimoto, R. G. Moore, I. I. Mazin, D. J. Singh, Z. Hussain, I. R. Fisher, and Z.-X. Shen, Phys. Rev. B **80**, 174510 (2009).
[19] B. Zhou, Y. Zhang, L.-X. Yang, M. Xu, C. He, F. Chen, J.-F. Zhao, H.-W. Ou, J. Wei, B.-P. Xie, T. Wu, G. Wu, M. Arita, K. Shimada, H. Namatame, M. Taniguchi, X. H. Chen, and D. L. Feng, Phys. Rev. B **81**, 155124 (2010).
[20] M. Yi, D. H. Lu, J. G. Analytis, J.-H. Chu, S.-K. Mo, R.-H. He, R. G. Moore, X. J. Zhou, G. F. Chen, J. L. Luo, N. L. Wang, Z. Hussain, D. J. Singh, I. R. Fisher, and Z.-X. Shen, Phys. Rev. B **80**, 024515 (2009).
[21] C. Liu, Y. Lee, A. D. Palczewski, J.-Q. Yan, T. Kondo, B. N. Harmon, R. W. McCallum, T. N. Lograsso, and A. Kaminski, arXiv:1006.0929 (unpublished).
[22] T. Kondo, A. F. Santander-Syro, O. Copie, C. Liu, M. E. Tillman, E. D. Mun, J. Schmalian, S. L. Budko, M. A. Tanatar, P. C. Canfield, and A. Kaminski, Phys. Rev. Lett. **101**, 147003 (2008).
[23] H. Eschrig, A. Lankau, and K. Koepernik, Phys. Rev. B **81**, 155447 (2010).
[24] C. He, Y. Zhang, B. Xie, X. Wang, L. Yang, B. Zhou, F. Chen, M. Arita, K. Shimada, H. Namatame, M. Taniguchi, X. Chen, J. Hu, and D. Feng, Phys. Rev. Lett. **105**, 117002 (2010).
[25] J.-Q. Yan, S. Nandi, J. L. Zarestky, W. Tian, A. Kreyssig, B. Jensen, A. Kracher, K. W. Dennis, R. J. McQueeney, A. I. Goldman, R. W. McCallum, and T. A. Lograsso, Appl. Phys. Lett. **95**, 222504 (2009).
[26] A. Jablonski, Surf. Interface Anal. **20**, 317 (1993).
[27] I. I. Mazin, M. D. Johannes, L. Boeri, K. Koepernik, and D. J. Singh, Phys. Rev. B **78**, 085104 (2008).
[28] F. J. Ma and Z.-Y. Lu, Phys. Rev. B **78**, 033111 (2008).
[29] D. J. Singh, Phys. Rev. B **78**, 094511 (2008).
[30] B. J. Kim H. Jin, S. J. Moon, J.-Y. Kim, B.-G. Park, C. S. Leem, J. Yu, T. W. Noh, C. Kim, S.-J. Oh, J.-H. Park, V. Durairaj, G. Cao, and E. Rotenberg, Phys. Rev. Lett. **101**, 076402 (2008).
[31] H. Cercellier, Y. Fagot-Revurat, B. Kierren, F. Reinert, D. Popović, and D. Malterre, Phys. Rev. B **70**, 193412 (2004).
[32] C. L. Yang, H. T. He, Lu Ding, L. J. Cui, Y. P. Zeng, J. N. Wang, and W. K. Ge, Phys. Rev. Lett. **96**, 186605 (2006).
[33] F. Chen, B. Zhou, Y. Zhang, J. Wei, H.-W. Ou, J.-F. Zhao, C. He, Q.-Q. Ge, M. Arita, K. Shimada, H. Namatame, M. Taniguchi, Z.-Y. Lu, J. Hu, X.-Y. Cui, and D. L. Feng, Phys. Rev. B **81**, 014526 (2010).
[34] Y. Zhang, B. Zhou, F. Chen, J. Wei, M. Xu, L. X. Yang, C. Fang, W. Tsai, G. H. Cao, Z. A. Xu, M. Arita, H. Hayashi, J. Jiang, H. Iwasawa, C. H. Hong, K. Shimada, H. Namatame, M. Taniguchi, J. P. Hu, and D. Feng, arXiv:0904.4022 (unpublished).
[35] C. Fang, H. Yao, W.-F. Tsai, J. P. Hu, and S. A. Kivelson, Phys. Rev. B **77**, 224509 (2008).
[36] J. Zhao, D.-X. Yao, S. Li, T. Hong, Y. Chen, S. Chang, W. Ratcliff II, J. W. Lynn, H. A. Mook, G. F. Chen, J. L. Luo, N. L. Wang, E. W. Carlson, J. Hu, and P. Dai, Phys. Rev. Lett. **101**, 167203 (2008).
[37] K. Matan, R. Morinaga, K. Iida, and T. J. Sato, Phys. Rev. B **79**, 054526 (2009).
[38] W. Yu, L. Ma, J. Zhang, G. Chen, T.-L. Xia, S. Zhang, and Y. Hou, arXiv:1004.3581 (unpublished).
[39] Y. Nakai, K. Ishida, Y. Kmihara, M. Hirano, and H. Hosono, J. Phys. Soc. Jpn. **77**, 073701 (2008).